Near-infrared imaging of liquid mixtures utilizing multi-channel photonic crystal wavelength filters

Masahiro Mitsuhashi, Yasuo Ohtera,* and Hirohito Yamada

Graduate School of Engineering, Tohoku University, Sendai 980-8579, Japan

**Corresponding author: ohtera@ecei.tohoku.ac.jp*

Received June 16, 2014; revised July 14, 2014; accepted August 5, 2014;
posted August 7, 2014 (Doc. ID 214076); published September 4, 2014

We demonstrate a near-infrared (NIR) spectroscopy-based real-time imaging system of aqueous alcohol solutions (ethanol containing water). The system obtains a set of NIR images by the combination of an InGaAs area sensor and four-channel patterned photonic crystal wavelength filters. Acquired pictures were decomposed into a set of NIR images and processed by principal component analysis (PCA). According to a preliminary experiment for water/ethanol mixture samples, we confirmed that the system was capable of identifying the mixture ratio with accuracy of the order of a few percentage points at a frame rate of approximately 24 frames per second (fps). © 2014 Optical Society of America

OCIS codes: (230.5298) Photonic crystals; (110.4234) Multispectral and hyperspectral imaging; (300.6340) Spectroscopy, infrared; (310.6628) Subwavelength structures, nanostructures.

http://dx.doi.org/10.1364/OL.39.005301

Near-infrared spectroscopy (NIRS) has become one of the most powerful tools for online process management and quality monitoring systems in various fields, such as agriculture [1], food industry [2], and gasoline and petroleum products industries [3,4]. The method has also played a key role in the biomedical monitoring of human bodies [5]. Relatively small light absorption in near-infrared (NIR) wavelengths has made it possible to acquire quality information inside the analyte without destroying or sampling it. In industrial fields, where the target product is semi-fixed, only a limited number of wavelength channels are usually sufficient to check the quality deviation. We anticipate imaging capability to experience the next technological advancement. A number of trials have been conducted to develop such multichannel NIRS imaging systems. Most of them consist of a NIR image sensor such as an InGaAs focal plane array and spectroscopic elements. Examples of the elements are (1) tunable wavelength filters (acousto-optic or liquid crystal [6]), (2) filter wheels [7], (3) diffraction gratings and diffractive optical elements [8], and (4) patterned wavelength filters [9].

Among these, the last element has several advantages over the others. It can capture multiple wavelength images with a single shot and can be constructed without moving parts and external driving circuits. Thus, it is suitable for moving, deforming, or time-varying targets. We have so far proposed and demonstrated multilayer-type photonic crystal wavelength filters (PhCFs) for this purpose. However, until now, the main focus has been to establish elementary design and fabrication technologies of the PhCF itself [10–13]. A feasibility study for the imaging systems has not been conducted yet.

In this study, we tried to demonstrate a proof-of-concept NIRS imaging experiment utilizing four-channel patterned PhCFs. Time-varying phenomena of practical targets were visualized in real time for the first time to the best of our knowledge. As a test target, we chose aqueous alcohol solutions (ethanol containing water). Noninvasive and remote monitoring of the mixture ratio of such a liquid is one of the major applications for NIRS in fields, such as bio-ethanol production lines, brewing processes of alcohol beverages, and postpackaging management of liquid products [14–16].

A schematic view of the PhCF is shown in Fig. 1. A wavy Si/SiO_2 multilayer was deposited on a patterned substrate by the autocloning method [17]. Details of the fabrication procedure were described in our previous works [11,13].

Figure 2 shows global and magnified views of the PhCF. The "M" region is the four-channel mosaic-patterned filter. Four miniature filter areas having a grating pitch (Λ) of 400, 440, 480, and 520 nm were periodically repeated in two dimensions. The distance between each filter is equal to the pixel pitch of the NIR camera to be used (30 μm). Figure 2(b) shows a microscopic image of the detail of the mosaic region. Each PhCF with a fixed aperture diameter (25 μm) is surrounded by a background PhCF, which has a grating pitch of 580 nm and serves as an all-stop filter. The film profile of the PhCF is as follows:

$$\text{air} - \text{AR}_{\text{top}} - (\text{LH})^8 - \text{AR}_{\text{bottom}} - \text{silica},$$
$$\text{L} = \text{SiO}_2\,(185\ \text{nm}), \text{H} = \text{Si}\,(185\ \text{nm}),$$
$$\text{AR}_{\text{top}} = \text{SiO}_2\,(203\ \text{nm}) - \text{Si}\,(152\ \text{nm}),$$
$$\text{AR}_{\text{bottom}} = \text{SiO}_2\,(188\ \text{nm}) - \text{Si}\,(168\ \text{nm}).$$

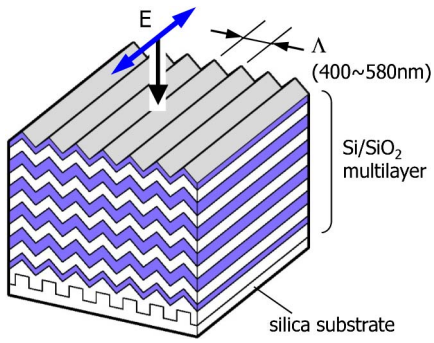

Fig. 1. Schematic view of the multilayer-type photonic crystal wavelength filter (PhCF).

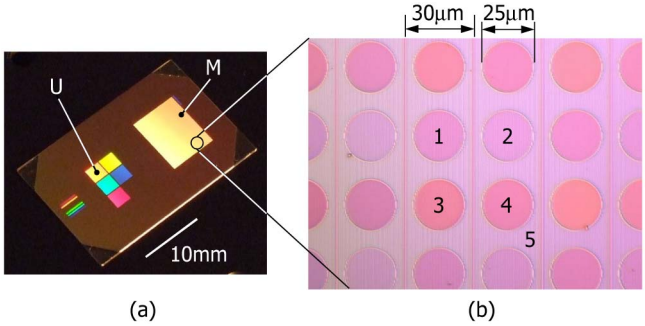

Fig. 2. Pictures of the fabricated filter. (a) Global view of the sample. U, uniform and wide-area PhCF region for transmittance evaluation; M, mosaic-patterned region for the imaging experiment. (b) Magnified image of the mosaic-patterned region. Miniature filters (1–4) have different transmission bands. Region 5 has the all-stop characteristic and was placed to suppress crosstalk of the adjacent pixels.

The main eight-period multilayer functions as a short-wave cut-edge filter [10]. The construction of the antireflective (AR) layers was designed using a simple parameter scanning method detailed in [12].

Transmittance for the TE wave (the electric field is parallel to the grooves of the gratings) was measured using the uniform PhCF region indicated as "U" in Fig. 2(a). The result is shown in Fig. 3(a). Transmittance in the passbands and stopbands was approximately 80 and <1%, respectively. Cut-off wavelengths were measured

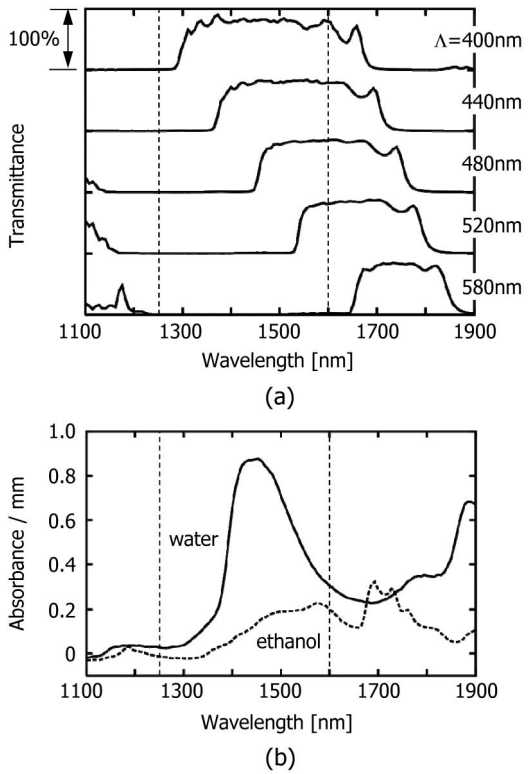

Fig. 3. Optical characteristics of the PhCF and the test target. (a) Measured transmittance of each PhCF. $\Lambda = 580$ nm corresponds to Region 5 of Fig. 2(b). (b) Absorbance of the water and ethanol. Dashed lines indicate the boundaries of the measuring band.

to be 1300, 1380, 1460, and 1540 nm for PhCFs 1–4, respectively, and 1675 nm for the all-stop filter.

We then tried to conduct NIRS imaging of water/ethanol mixtures. Liquid samples of various ethanol molar fractions and two kinds of optical path lengths ($d = 1$ and 2 mm) were prepared. Examples of their absorption spectra are shown in Fig. 3(b). Note that both pure and ethanol-included water have broad absorption bands in the vicinity of $\lambda \sim 1450$ nm [15,18]. The PhCFs were designed to cover this band. The dashed vertical lines in Figs. 3(a) and 3(b) indicate the wavelength band of interest in this experiment.

The experimental setup for the liquid discrimination is shown in Fig. 4. Long-pass (Thorlab Inc., FEL1250) and short-pass (Edmund Optics Co. Ltd., No. 84656) filters were used to cut $\lambda < 1250$ nm and $\lambda > 1600$ nm spectral components, respectively. The image of a liquid-filled glass cell was first focused on the PhCF and then transferred to the NIR camera (Allied Vision Technologies NIR-300PCL, 320×256 pixels, pixel pitch of 30 μm, 12-bit resolution, CameraLink interface) by a telecentric relay lens (OPTART Inc., TCLF1000-F). Data were then passed to a personal computer (PC) via a frame grabber board (AVAL Data Inc., APX-3316).

Prior to imaging, we adjusted the pixels of the PhCF and NIR camera. First, a magnified view around the four corners of the PhCF was displayed. By monitoring this, the angle and position of the PhCF were coarsely aligned. Then, we displayed the distribution of difference of light intensities between adjacent pixels. The PhCF position and the magnification of the telecentric lens were finely adjusted by maximizing the intensity contrast.

The procedure of data analysis is as follows. In summary, we carried out principal component analysis (PCA) [19] at both preprocessing and main processing of the imaging routine. The latter was carried out in every picture frame.

(Preprocessing: executed only once before entering the video capturing)

1. A standard white diffuse plate was pictured by a NIR camera through PhCF. The light intensities corresponding to the four-channel PhCFs are R_1–R_4.
2. Still pictures of the sample (various concentration and thickness) were captured. The intensities are denoted by P_1–P_4, respectively. These data were used for calibration.
3. $P_1 - P_4$ were normalized and converted to the average absorbance; i.e., $A_i = -\log_{10}(P_i/R_i)$ $(i = 1 \text{ to } 4)$.

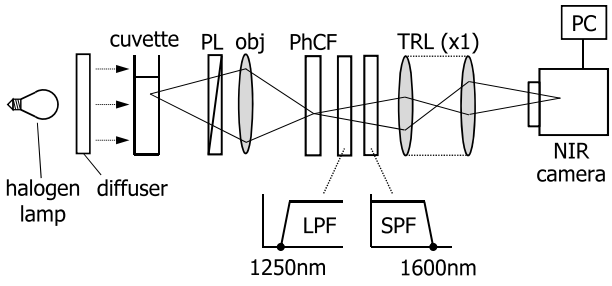

Fig. 4. Experimental setup for the imaging experiment. PL, polarizer; obj, objective lens; TRL, telecentric relay lens; LPF and SPF, long-pass and short-pass filters.

4. PCA was applied to the set of A_i. Loading vectors were found.

5. A new set of PC axes (PC'_1 and PC'_2) were defined by rotating the original PC_1 and PC_2 axes by 4.47 degrees counterclockwise so that they corresponded to ethanol concentration and thickness, respectively. PC'_1 and PC'_2 were finally expressed as a linear combination of A_i as follows:

$$PC'_1 = 0.500A_1 + 0.626A_2 + 0.448A_3 + 0.397A_4,$$
$$PC'_2 = -0.375A_1 - 0.451A_2 + 0.454A_3 + 0.671A_4.$$

(Main processing)

1. Four kinds of light intensities ($I_1 - I_4$) were acquired by picturing the samples through four PhCFs.

2. I_i was normalized by R_i (already stored at preprocessing) at each pixel and converted to absorbance $A_i = -\log_{10}(I_i/R_i)$ ($i = 1$–4).

3. PC scores were calculated using the previous equations.

The main processing was executed in real time. PC scores at each position on a sample were obtained using the intensities of every four pixels (2×2, PhCFs 1–4) at every picture frame.

A summary of the PCA score plot is shown in Fig. 5. Each bar-like cluster consists of the PCs obtained from central 16×16 units (32×32 pixels) of the NIR camera.

For a $d = 1$ mm cell, the PC'_1 score range of $0.18 \le PC'_1 \le 0.62$ was linearly mapped to 0%–100% of an ethanol molar fraction. Similarly, for a $d = 2$ mm cell, $0.38 \le PC'_1 \le 0.99$ was linearly mapped to an ethanol fraction of 0%–100%.

The approximate calibration functions for the ethanol fraction (c) are expressed as follows. These scales are indicated at the upper part of Fig. 5(b)

$$c = \begin{cases} 229PC'_1 - 41.7 & \%(d = 1\text{ mm}, PC'_2 < 0.075) \\ 164PC'_1 - 62.5 & \%(d = 2\text{ mm}, PC'_2 > 0.075) \end{cases}.$$

For the current frame rate, the full width of the noise intensity was measured to be approximately 9.8—out of the 0–4095 (12-bit) digital signal range. This noise was overridden to the average signal count of 1400–2500 (depending on the PhCF channel). The error of ethanol concentration can then be estimated by the error of the PC'_1 score. Using the previous numbers, the error was calculated as approximately 3.1% for a water-rich sample to 4.9% for an ethanol-rich sample. This is the base for the dispersion (or detectable resolution) in Fig. 5. However, the path length was found to be recognized with ~0.5 mm resolution.

We then tried to visualize the mixture process of two pure liquids in real time using the previous calibrations. Two cases were demonstrated: (1) pure water injected into an ethanol-filled cell and (2) pure ethanol injected into a water-filled cell. The two liquids were immediately mixed for (1) but almost kept separate for (2) if slowly and carefully injected. Figure 6 shows a pseudocolor representation of the ethanol molar fraction for (1) with a cell thickness of $d = 1$ mm. Note that pixels with an

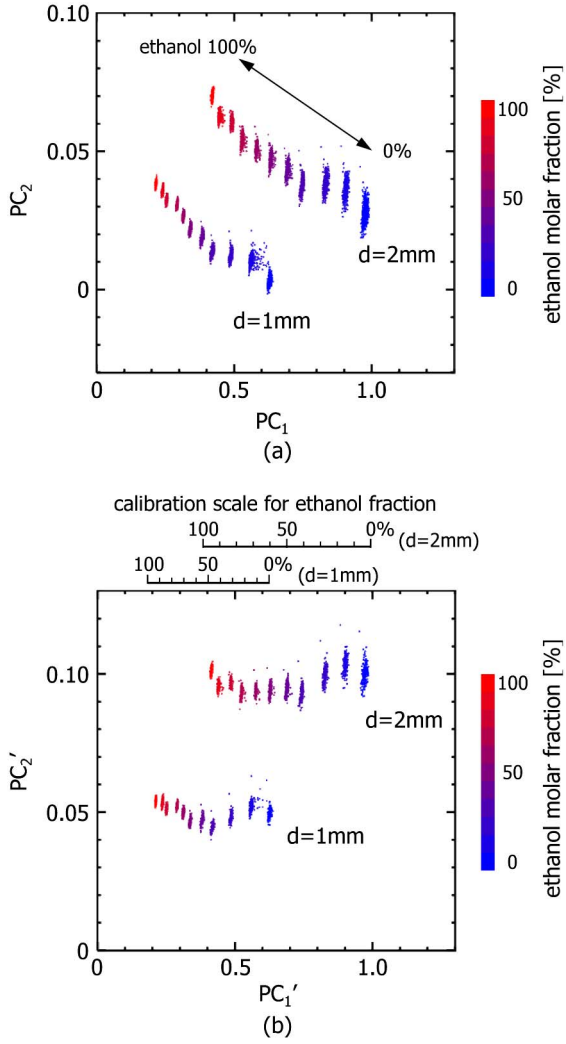

Fig. 5. Principal component analysis (PCA) score plot. (a) Original plot. (b) Plot after axes rotation. Original axes were rotated by 4.47 deg counterclockwise to correlate the new PC'_1 and ethanol concentration.

estimated ethanol fraction of less than 0% or more than 100% are black, which means that they are out of range. As shown in the figure, a complex microscopic distribution was clearly observable during the rapid mixing process. The frame rate was approximately 24 frames per second (fps). The time resolution was thus approximately 42 m/s. Note that the free-running frame rate of the NIR camera was approximately 50 fps. Thus, the main PCA calculation routine spent almost half

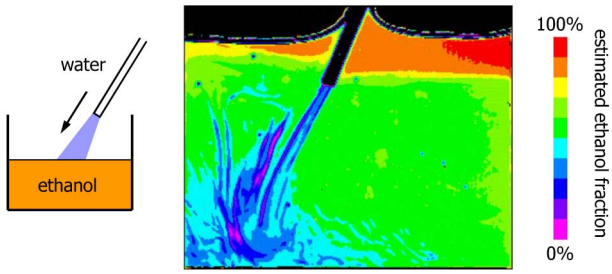

Fig. 6. Map of estimated ethanol fraction (Media 1). Water was injected into an ethanol-filled cuvette ($d = 1$ mm).

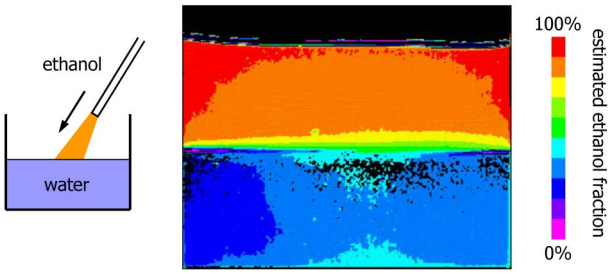

Fig. 7. Map of estimated ethanol fraction (Media 2). Ethanol was slowly poured into a water-filled cuvette ($d = 1$ mm).

of the repetition period. However, it did not affect the live video capturing because the arithmetic operations per frame were limited (division, logarithm, and multiplication).

Figure 7 shows the distribution for (2). Here, the detail of the boundary between the two liquids is clearly visualized. The boundary was found to be stable and remained this way if water was poured slowly from the edge of the cell. We also observed that the interface gradually spread as time passed of the order of 10 min.

Finally, we would like to discuss the further development potential of the PhCF technology. One needs at least several lattices for the periodic structure to exhibit photonic crystal-specific characteristics. If the number is small, its spectral characteristic diverges from the ideal crystal. Thus, the minimum lateral size of PhCF for the current application may be 4–6 μm if one PhCF consists of 10 lattices. Considering that the typical pixel pitch of today's NIR focal plane array is 25–30 μm, we can say that this size is sufficiently small. However, if the multilayer was designed as a bandpass function, the minimum attainable bandwidth is of the order of 50–175 nm [13]. Their cut-off wavelengths can be adjusted by a resolution of approximately 10 nm [11] (depending on the resolution of lithography). Therefore, our PhCF is suitable for discriminating NIR absorption spectra that exhibit a moderate spectral change over a wavelength range of a few tens of nanometers.

In conclusion, we constructed a four-channel NIRS imaging setup utilizing PhC patterned wavelength filters and a NIR camera. As a result of a proof-of-concept experiment, both rapid and slow variation processes of a liquid sample were visualized. Improvement of the image quality will be the subject of future experiments by implementing flame accumulation and deconvolution.

This research has been supported by the Asahi Glass Foundation. The PhCF fabrication process was carried out in the PCR facility of RIEC, Tohoku University.

References

1. G. D. Batten, J. Near Infrared Spectrosc. **6**, 105 (1998).
2. G. Downey, J. Near Infrared Spectrosc. **4**, 47 (1996).
3. G. Bohács and Z. Ovádi, J. Near Infrared Spectrosc. **6**, 341 (1998).
4. J. Workman, Jr., J. Near Infrared Spectrosc. **4**, 69 (1996).
5. F. F. Jöbsis, Science **198**, 1264 (1977).
6. H. R. Morris, C. C. Hoyt, and P. J. Treado, Appl. Spectrosc. **48**, 857 (1994).
7. K. J. Brodbeck, A. E. Profio, and T. Frewin, Med. Phys. **14**, 637 (1987).
8. E. Herrala, T. Hyvarinen, O. Voutilainen, and J. Lammasniemi, Sens. Actuators **A61**, 335 (1997).
9. N. S. Gluck, R. B. Bailey, R. de la Rosa, and R. L. Hall, Appl. Opt. **35**, 5520 (1996).
10. Y. Ohtera, T. Onuki, Y. Inoue, and S. Kawakami, J. Lightwave Technol. **25**, 499 (2007).
11. Y. Ohtera, D. Kurniatan, and H. Yamada, Appl. Opt. **50**, C50 (2011).
12. Y. Ohtera, K. Daniel, and H. Yamada, Opt. Express **18**, 12249 (2010).
13. Y. Ohtera and H. Yamada, Opt. Lett. **38**, 1235 (2013).
14. B. Liebmann, A. Friedl, and K. Varmuza, Anal. Chim. Acta **642**, 171 (2009).
15. S. Engelhard, H.-G. Löhmannsröben, and F. Schael, Appl. Spectrosc. **58**, 1205 (2004).
16. N. W. Broad, R. D. Jee, A. C. Moffat, M. J. Eaves, W. C. Mann, and W. Dziki, Analyst **125**, 2054 (2000).
17. T. Kawashima, Y. Sasaki, K. Miura, N. Hashimoto, A. Baba, H. Ohkubo, Y. Ohtera, T. Sato, W. Ishikawa, T. Aoyama, and S. Kawakami, IEICE Trans. Electron. **E87-C**, 283 (2004).
18. G. M. Hale and M. R. Querry, Appl. Opt. **12**, 555 (1973).
19. R. Kramer, *Chemometric Techniques for Quantitative Analysis* (CRC, 1998).